# Designing multifunctional enzymatic devices for biosensing and chemical conversion

Wei, Z.

**Publication date**
2025

# *Chapter 2.*

# *Engineered enzymes for improving the stability of electrochemical biosensors*

Part of this chapter was published as "A high-performance electrochemical biosensor using an engineered urate oxidase", Z. Wei, T. Knaus, Y. Liu, Z. Zhai, A. F. G. Gargano, G. Rothenberg, N. Yan and F. G. Mutti, *Chem. Commun.*, **2023**, 59, 8071. DOI: 10.1039/D3CC01869E.

Scan me for the published paper.

## 2.1. Abstract

We constructed a high-performance biosensor for detecting uric acid by immobilizing an engineered urate oxidase on gold nanoparticles deposited on a carbon-glass electrode. This biosensor showed a low limit-of-detection (9.16 nM), a high sensitivity (14 μA/μM), a wide range of linearity (50 nM – 1 mM), and more than 28 days lifetime.

## 2.2. Introduction

Biosensors based on oxidoreductase enzymes were intensively studied during the last decade due to the requirement for more rapid and precise diagnosis protocols.[1-3] However, naturally (i.e., wild-type) available oxidoreductases are often unstable at high temperatures, leading to narrower operating conditions of the enzyme-based biosensing platforms and restricted applications.[4,5] Therefore, several methods were proposed for increasing the thermal stability of enzymes within biosensors. The most frequently employed strategy in the field of biosensing consists in the encapsulation of the enzymes into porous network materials or the immobilization on nanofibers.[6,7] The confinement of the enzymes can physically protect them from the outside hyperthermia and reduce their exposure to the potentially harsh environment. Furthermore, the structural stability of enzymes can be enhanced through coordination and intermolecular interactions inside the cage.[8] However, the protection conferred by these materials has the disadvantage to decrease the actual catalytical activity of enzymes due to the reduced accessibility of analytes and the possible occupation of the active sites by the inner materials. [9] Consequently, this methodology sacrifices catalytic performance to improve thermal stability, which is not ideal for the development of more efficient biosensing platforms. In view of this, a rational strategy would be expected that can endow enzymes with both high thermal stability and outstanding catalytical activity.

Structural-guided enzyme engineering with the aid of computational methods or the directed evolution of an enzyme can provide a solution to this dilemma by increasing the enzyme stability (e.g., thermal, pH, additives) while retaining of even enhancing the catalytical efficiency.[10-14] The specificity of the enzyme toward a substrate or a cofactor can also be optimized along with its regioselectivity, and stereoselectivity in some catalytic reactions.[15,16] Thermal stabilization can also be enhanced by introducing salt bridges and/or disulfide bonds.[17] Thus, protein engineering can improve the catalytic efficiency of enzymes for existing as well as new electrochemical biosensors.

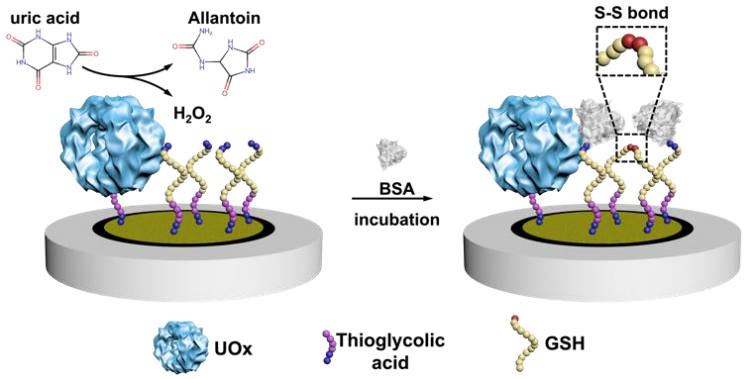


**Scheme 1.** The principle of the electrochemical UA biosensor.

Here, we constructed an electrochemical biosensor that harnessed the performance of a thermostable engineered enzyme, which was further modified in our group by genetically fusing a poly-histidine purification tag. As the essential biomarker for gout, uric acid (UA) was selected as the model analyte and we used urate oxidase (UOx) as the model enzyme in this study.[18,19] UOx catalyzed the oxidation UA to yield $H_2O_2$[20] as a secondary product, which then promoted the covalent immobilization of bovine serum albumin (BSA) onto electrodes through the formation of the disulfide bond between BSA and glutathione (GSH, see Scheme 1 and Scheme 2).[21]

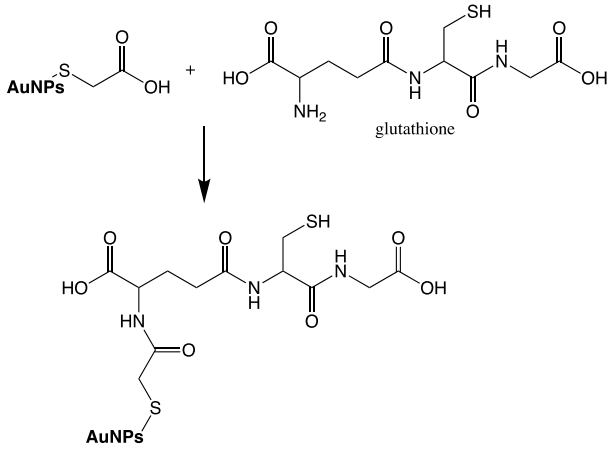


**Scheme 2**. The mechanism for the formation of the covalent bond between glutathione (-$NH_2$ group) and thioglycolic acid (-COOH group).

## 2.3. Results and discussion

### 2.3.1. Recombinant expression and purification of engineered UOx

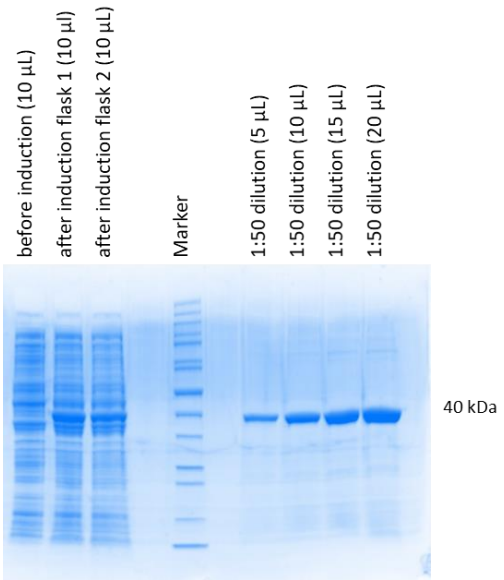


**Figure 1.** SDS-Page analysis for the expression of UOx R298C (engUOx) and of the purified protein. Marker: PageRuler™ Unstained Protein Ladder (Thermo Fisher Scientific).

The engineered UOx from *Bacillus* sp. TB-90 (BTUO R298C, herein noted as engUOx) was recombinantly produced in *E. coli* as His-tagged protein and purified by $Ni^{2+}$-affinity chromatography in our group (Figure 1).[4,22] The reported substitution of the arginine 298 residue with a cysteine enables the spontaneous formation of an inter-subunit disulfide bond and significantly improved the thermo-stabilization of the enzyme (Figure 2A). Additionally, this single point mutation did not result in any negative influence on the catalytical performance and eliminated the need for adding sulfate salt to stabilize the enzyme.[17]

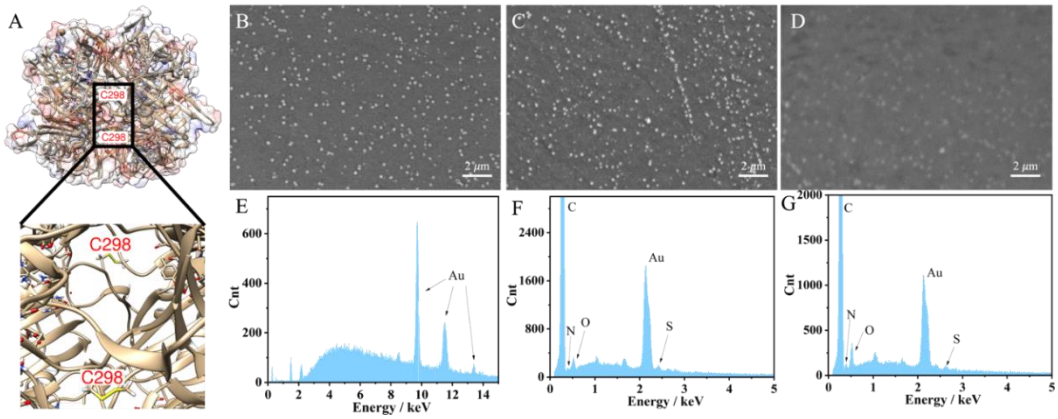


**Figure 2.** Structure of engUOx and characterizations of the biosensor. (A) 3D structure of engUOx highlighting the inter-subunit disulfide bonds. SEM images of electrochemically deposited AuNPs on GCE (B), incubated with engUOx (C), and incubated with UA and BSA (D). EDS images of electrochemically deposited AuNPs on GCE (E), incubated with engUOx (F), and incubated with UA and BSA (G).

### 2.3.2. Principle of UA electrochemical biosensor

After producing the enzyme, we built the electrochemical UA biosensor in a stepwise manner (Scheme 1, for more details see Scheme 2). We deposited the gold nanoparticles (AuNPs) on the electrode by electroreduction as developed in previous work.[23] Next, thioglycolic acid was added, forming Au-S bonds. The thioglycolic acid molecules, upon activation of the carboxyl groups, served as linkers to the engUOx by forming amide bonds. To further amplify the electrochemical signal, the electrode was decorated with sulfhydryl groups by attaching GSH, and BSA was selected as the impedance probe. When the UA is added, engUOx catalyzes UA oxidation and yields $H_2O_2$ as a by-product. This $H_2O_2$ reacts further, generating a disulfide bond between BSA and GSH, changing the conductivity and thereby the current of the electrochemical UA biosensor.

### 2.3.3. Characterization of the UA biosensor

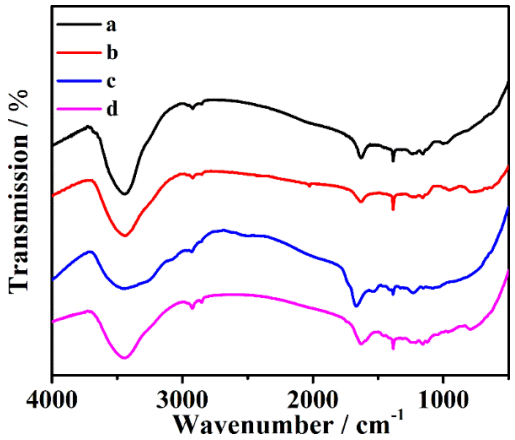


**Figure 3.** FT-IR spectrum of deposited AuNPs on the electrode (a), immobilized with engUOx (b), incubated with blocking agents (c), and incubated with UA and BSA solution (d).

This stepwise process was characterized to ensure the successful implementation. Scanning transmission microscopic (SEM) image clearly showed the deposited AuNPs on the surface of the electrode with a uniform distribution (Figure 2B) while the image became less defined upon incubation with the engUOx due to the reduced conductivity of the electrode's surface (Figure 2C). The energy dispersive X-ray (EDS) spectrum also evidenced the successful immobilization of engUOx, showing two new peaks of N and S atoms from the enzyme (Figure 2F), which are not detected for the pure Au-deposited electrodes (Figure 2E). Fourier transform infrared spectroscopy (FTIR) results also supported the successful construction of the biosensor (Figure 3). After attaching the BSA, the SEM image became blurry (Figure 2D) and the ratio of the intensity of the N and S peaks versus Au peak in EDS spectrum increased (Figure 2G). This shows that more protein was anchored on the electrode's surface. In the FTIR spectrum, we could observe the disulfide bond that confirmed the occurrence of the reaction between BSA and GSH in the presence of $H_2O_2$ (Figure 3). In a separated experiment, we also demonstrated that the BSA can be linked to GSH by the oxidative reaction in presence of $H_2O_2$. In fact, when BSA (66428 Da) and GSH were incubated in presence of $H_2O_2$, a molecular weight increase was observed by size-exclusion chromatography-mass spectrometry (SEC-MS: BSA+GSH 66734 Da; Figure 4).

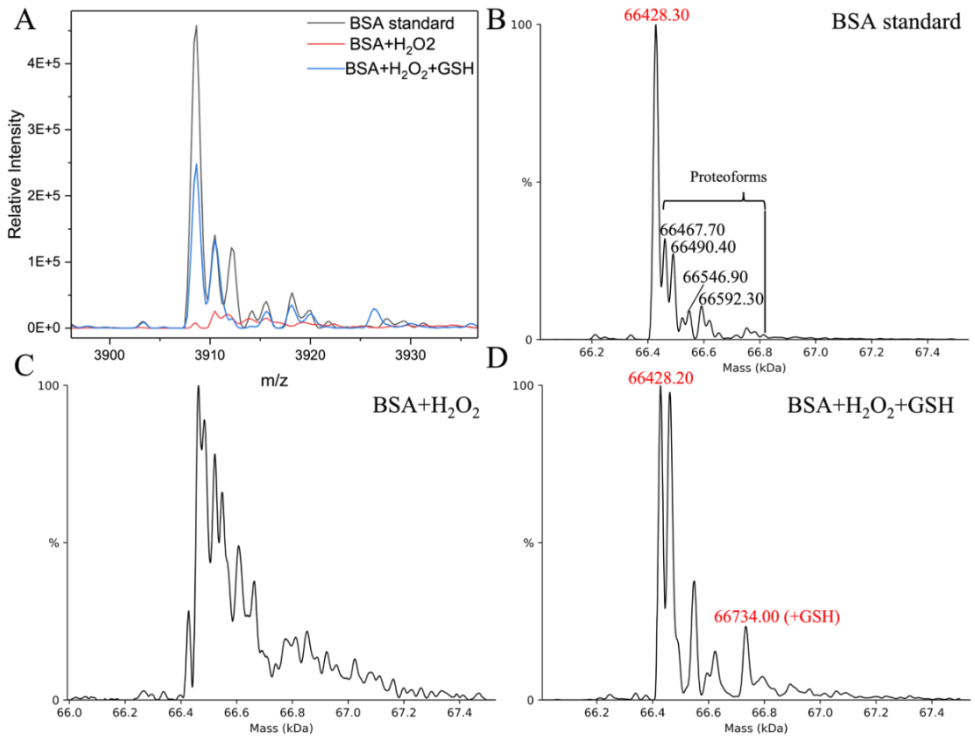


**Figure 4.** Comparison of the most abundant charge state MS spectrum (+17) for BSA (bovine serum albumin) protein: reference BSA, BSA exposed to H2O2, and BSA exposed to both H2O2 and GSH (A). Deconvoluted MS spectra of pure BSA (B), BSA reacted with H2O2 (C), and BSA reacted with H2O2 and GSH (D). In the presence of GSH, a peak at 66734.00 Da was observed. With the deconvolution results, the BSA standard has different proteoforms, among which 66428.20 Da was the most abundant. After being treated with H2O2, the BSA was oxidized, leading to a complex heterogeneous mixture of oxidized species. In the presence of GSH, a new peak at 66734.00 Da was observed after the reaction, which confirms the linkage between GSH (mass 307.33 Da) and BSA. The error in ppm of the GSH assignment is of 7.10 ppm (error= $\frac{Mass_{theory}-Mass_{observed}}{Mass_{theory}}$ *10^6= $\frac{(66428.20+307.33-2)-66734.00}{66428.20}$ =7.10 ppm) which reflects a good accuracy in the modification of a 66 kDa molecule.

### 2.3.4. Stepwise establishment of the UA biosensor

The characterization of the stepwise procedure for the fabrication of the UA biosensor was also performed electrochemically by cyclic voltammetry (CV, Figure 5A). Compared to bare electrodes, the electrodes deposited with AuNPs had higher current response because AuNPs are good conductive materials. After the covalent derivatization with the thioglycolic acid, the current value decreased due to the poor conductivity of the added organic molecule, thus demonstrating that the thioglycolic acid was successfully linked to AuNPs. Next, the similar behavior was observed after engUOx and GSH were immobilized on electrode, respectively. These observations confirmed that engUOx and GSH were successfully immobilized on the electrodes.

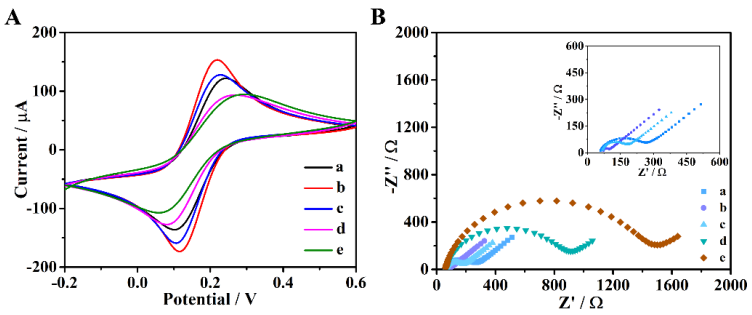


**Figure 5.** CV (A) and EIS (B) of different modified electrodes: bare electrode (curve a), AuNPs/GCE (curve b), thioglycolic acid/AuNPs/GCE (curve c), incubated with engUOx (curve d), blocked with GSH (curve e).

To further characterize the construction procedure, we conducted electrochemical impedance spectroscopy (EIS) to monitor the impedance of the biosensing interface (Figure 5B). The non-Ohmic charge transfer impedance was monitored by quasi-semicircle diameter of the Nyquist plots. Compared with bare electrode (curve a), the electrodes decorated with AuNPs (curve b) had smaller diameter due to the good conductivity of gold material. After incubating with thioglycolic acid, the diameter of the semicircle increased a little (curve c), which indicated that thioglycolic acid was successfully linked on the electrodes. The impedance of the biosensing platform increased gradually upon engUOx (curve d) and GSH (curve e) immobilization. This electrochemical characterization also indicated that the UA biosensing platform was successfully constructed.

### 2.3.5. Optimization of biosensing platform

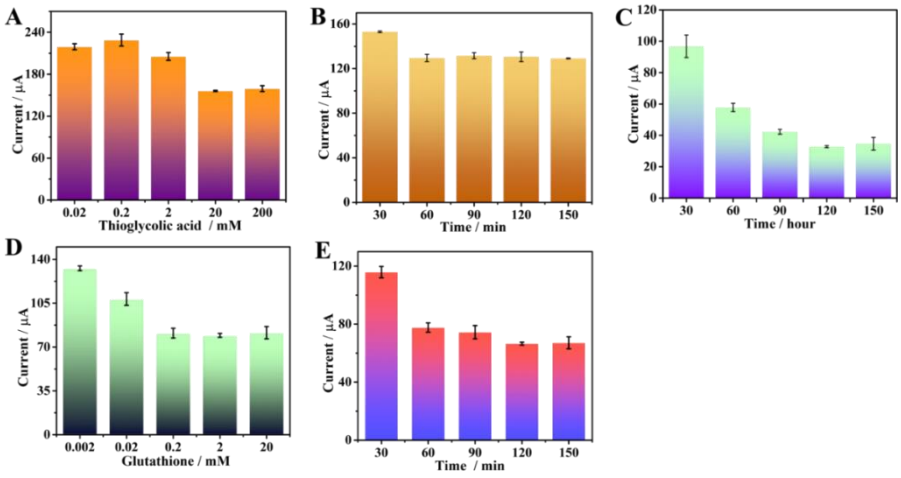


**Figure 6.** Effect of the concentration of thioglycolic acid (a), incubation time of thioglycolic acid (b), incubation time of engUOx (c), concentration of GSH (d), and catalytic reaction time on the SWV responses. Error bars represent standard deviations of three experiments in parallel.

We then studied the influence of different parameters on the performance of the

biosensor, comprising concentration of thioglycolic acid and glutathione, incubation time for them, and the catalytic reaction time (Figure 6). Judging by the square wave voltammetry (SWV) response, the obtained optimum conditions were used for the continuation of this work.

### 2.3.6. Biosensing assays with engUOx for UA detection

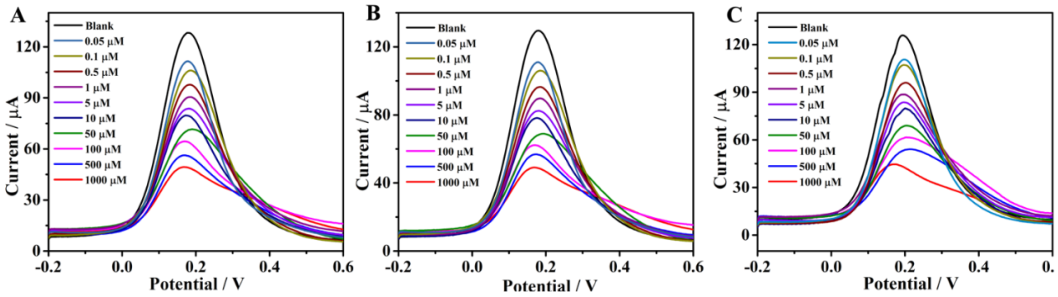


**Figure 7.** The performance of electrochemical UA biosensor with engUOx. SWV responses of electrochemical detection for UA (three independent determinations).

We quantitatively evaluated the sensing performance with a specific focus on the limit of detection (LOD), linear detection range, selectivity, and reliability. The current in square wave voltammetric test (SWV) decreased at increasing concentration of UA (Figure 7) and a linear relationship was observed between the current difference value (ΔI) and the logarithm of the UA concentrations in the range of 0.05–1000 μM (Figure 8).

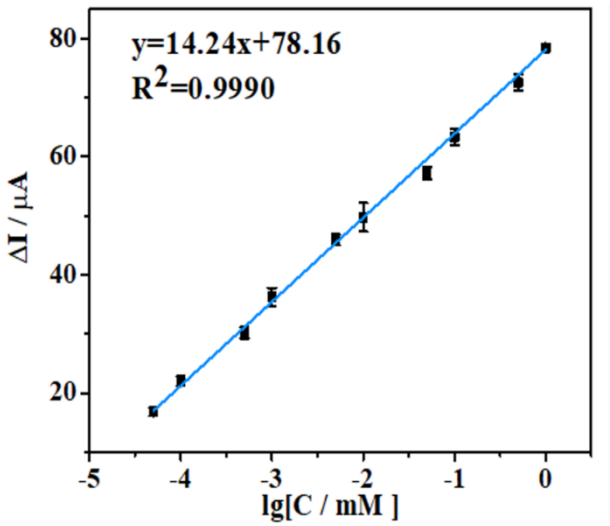


**Figure 8.** The calibration plot between the ΔI (-0.251 V vs. Ag/AgCl) and the logarithm values of UA concentrations for engUOx (the error bars denote standard deviations for n=3).

According to the literature data, the concentration of uric acid in the serum of healthy individuals ranges from ca. 210 μM to ca. 430 μM for adult men and from ca. 150 μM

to ca. 360 μM for adult women. Uric acid concentration above these thresholds are critical for the diagnose of renal hyperuricemia and gout.[24] In other physiological samples like sweat, the concentration of uric acid was determined to be as ca. 25 μM.[25] Therefore, we can conclude that the biosensor developed in this work is suitable for determination of uric acid concentration in real samples. The LOD was calculated to be 9.16 nM, comparable with other UA biosensors described in previous reports. Linearity range and LOD values for the most common UA biosensors are reported Table 1 (and references herein).

**Table 1.** Comparison of the detection performance of reported UA biosensor.

| Entry | Types of sensors | Linear range | LOD | Reference |
|---|---|---|---|---|
| 1 | Fluorescent | 0.01−400 μM | 2.3 nM | Qu et[26]. |
| 2 | Electrochemical | up to 700 μM | 0.066 μM | Jain et[27]. |
| 3 | Organic electrochemical transistors | 50−1000 μM | 4.5 μM | Galliani et[28]. |
| 4 | Electrochemical | 25−2500 μM | 0.023 μM | Wnag et[29]. |
| 5 | Electrochemical | 50–2000 μM | 0.019 μM | Ahmad et[30]. |
| 6 | Electrochemical | 5−100 μM | 0.33 μM | Shi et[31]. |
| 7 | Electrochemical | 0.01−0.145 μM | 6 nM | Abbas et[32]. |
| 8 | Electrochemical | 0.05−1000 μM | 9.16 nM | This work |

Notably, biosensors possessing a similar LOD value exhibit a narrower range of linearity, thus making them not broadly applicable for the determination of uric acid in real serum samples (Table 1 entries 1 and 7). Moreover, owing to the characteristic specificity of the enzymes, our biosensor showed outstanding selectivity to UA in presence of different interferents (Figure 9A and Table 2). Since our UA biosensor operates with BSA as impedance probe, a sample containing only BSA produced the highest current of ca. 120 μA, which can be considered as the background. Samples containing BSA and each of the interferents at 1 mM concentration produced a negligible variation of the current, likely due to a small variation of the non-specific BSA absorption on the electrode's surface as known in the literature.[33-35] In contrast, the UA sample measured at 10-fold lower concentration (100 μM) produced a great decrease of the current value (ca. 60 μA). Moreover, a sample obtained by mixing all the interferents (1 mM, each) with UA (100 μM) produced the same current as for a sample with UA alone (100 μM). These data demonstrates the high selectivity over competition for our UA biosensor, in agreement with the literature.[36] Finally, the reliability of our biosensor was evidenced by measuring standard samples, since a

regression coefficient of 0.9998 was calculated (Figure 9B).

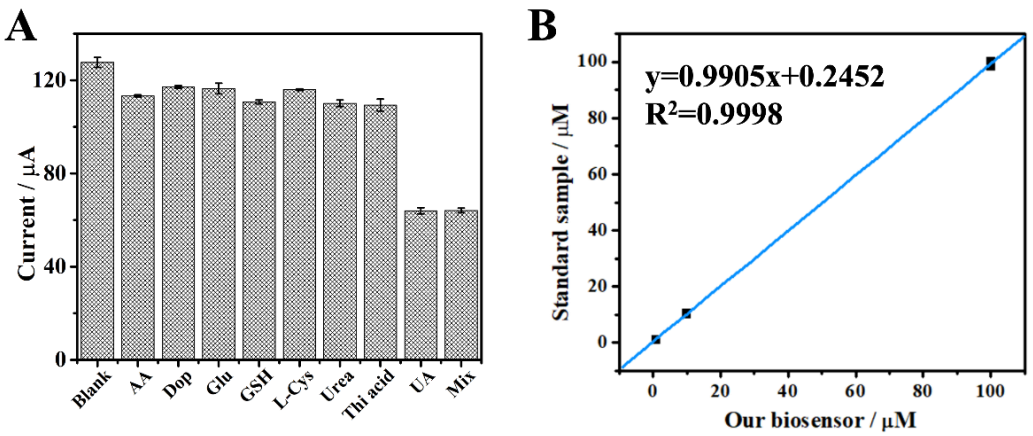


**Figure 9.** (a) Current responses measured to assess the specificity of the UA biosensor. The concentration of the interferent was set at 1 mM in each sample (AA: ascorbic acid; Dop: dopamine; Glu: glutamic acid; l-Cys: l-cysteine; Urea; Thi acid: thioglycolic acid). The concentration of uric acid sample (UA) was set at 100 μM. The mixture sample (Mix) consisted of all the interferents (1 mM, each) and UA (100 μM). Blank is a sample containing only BSA. (b) The concentration result obtained from our biosensor vs standard samples. The error bars are standard deviations for n = 3.

### 2.3.7. The advantage engUOx biosensing platform

To prove the advantage of using engUOx within our biosensing platform, we constructed the same type of biosensor using the same procedure but with a commercial UOx (a wild-type enzyme from *Candida* sp.). Figure 4 depicts the comparison of the biosensing performance between engUOx and the commercially available UOx. Upon incubation with UA solution, we measured a ΔI current value decreased of 15.44 μA for commercial UOx-based biosensor and of 63.80 μA for engUOx-based biosensor (Figure 10A and 10B). These results implied that engUOx leads to a greater current change than commercial UOx in electrochemical biosensing process at the same conditions. We infer the higher sensing performance of engUOx compared with the commercial UOx to the higher stability of the former, so that a higher fraction of the enzyme can retain a high catalytic activity during the incubation. In fact, the engUOx used in this work originates from *Bacillus* sp. that is a thermostable soil bacterium.[17] In contrast, the commercial UOx originates from *Candida* sp. that is a yeast.[37] Enzymes from thermophilic bacteria are commonly more stable than from eukaryotes. Furthermore, engUOx was further stabilized by adding a sulfur-sulfur inter-subunit bridge.[17] Finally, engUOx and the commercial UOx have a low sequence identity (24%) that supports the different catalytic behavior (for sequence alignment: Method part, section 1.10).

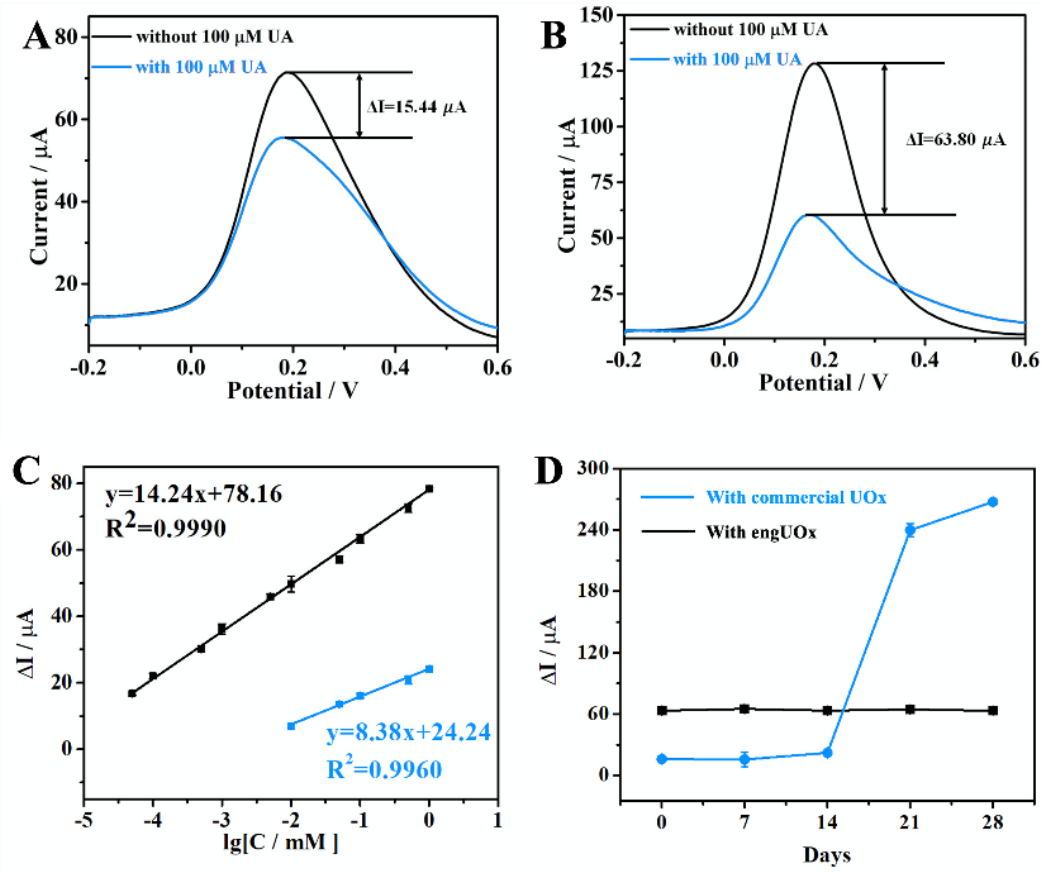


**Figure 10.** Superior biosensing performance of engUOx compared with commercial UOx. SWV current signal difference of the biosensor constructed with commercial UOx (A) and engUOx (B). (C) The calibration plot between the ΔI (-0.251 V vs. Ag/AgCl) and the logarithm values of UA concentrations obtained for engUOx (black) and commercially available UOx (blue). (D) Comparison of the life-time stability of our biosensing platform using either engUOx or commercial UOx; stability was monitored as SWV current responses. The error bars denote standard deviations for n = 3.

As a result, our biosensor performed better when using engUOx than conventional, commercial UOx (LOD = 5110 nM). Notably, the LOD was thousand-fold lower and the linear range was hundred-fold higher for the biosensor with engUOx compared with the same with commercial UOx. The sensitivity of UA biosensor with engUOx (14.24 $\mu A[\log C_{UA}]^{-1}$) was almost two-fold higher than the one with commercial UOx (8.38 $\mu A[\log C_{UA}]^{-1}$), which allows for a more precise quantification of UA with the former (Figure 10C). Finally, we also compared the life-time of our biosensing platform using either engUOx or commercial UOx. The biosensor fabricated with engUOx exhibited at least twice longer life-time than that of the biosensor fabricated with commercial UOx (Figure 10D). Therefore, our biosensor for UA detection based on engUOx has favorable storage properties that makes it suitable for real-world application.

**Table 2.** The current response of interfering chemicals

| Interference | Con (μM) | Current (μA) | Average (μA) | Standard deviation |
|---|---|---|---|---|
| Blank | 0 | 129.6<br>128.2<br>125.4 | 127.7 | 2.139 |
| Ascorbic acid | 1000 | 113.8<br>112.9<br>113.3 | 113.3 | 0.4510 |
| Dopamine | 1000 | 117.3<br>116.5<br>117.6 | 117.1 | 0.5690 |
| Glucose | 1000 | 117.9<br>117.7<br>113.8 | 116.5 | 2.312 |
| Glutathione | 1000 | 109.8<br>110.9<br>111.4 | 110.7 | 0.8190 |
| L-cysteine | 1000 | 115.7<br>116.4<br>116.0 | 116.0 | 0.3510 |
| Urea | 1000 | 108.9<br>110.0<br>111.6 | 110.1 | 1.358 |
| Thioglycolic acid | 1000 | 107.1<br>108.8<br>112.2 | 109.3 | 2.597 |
| Uric acid | 100 | 62.50<br>64.40<br>65.00 | 63.97 | 1.305 |
| Mix solution | UA 100<br>Others<br>1000 | 65.25<br>63.92<br>63.28 | 64.16 | 1.010 |

## 2.4. Conclusion

In summary, we have designed and developed a biosensing platform for the highly sensitive and reliable detection of UA within a wide linear range of concentrations. The method takes advantage of the covalent immobilization of the UOx on Au-NP deposited on a glass-carbon electrode through the linkage using thioglycolic acid and EDC chemistry. The derivatization of the electrode surface with GSH and using BSA as an

impedance probe is crucial for achieving the high biosensing performance. Moreover, the use of an engineered and highly thermostable UOx (engUOx) afforded greater biosensing performance, stability and life-time compared with the use of commercial UOx. This work shows how the performance of electrochemical biosensors can be improved by implementing engineered enzymes. It also reiterates the effectiveness of biochemical technique in advancing the biosensing field and provides a robust strategy for the evolution of similar sensors.

## 2.5. Methods

### 2.5.1. Materials and equipment

Hydrogen tetrachloroaurate (III) hydrate ($HAuCl_4.3H_2O$), ascorbic acid (AA, 99.7%), $K_2Fe(CN)_6$, uric acid (UA), ammonium acetate, glutathione (GSH), urea, N-hydroxysuccinimide (NHS), dopamine (Dop), cysteine (l-Cys) and bovine serum albumin (BSA) and commercial urate oxidase from *Candida* sp. were purchased from Sigma-Aldrich (Darmstadt, Germany). KCl and $KH_2PO_4$ were purchased from Merck (Darmstadt, Germany). D-Glucose was purchased from Fisher. Thioglycolic acid and N-(3-Dimethylaminopropyl)-N′-ethylcarbodiimide hydrochloride (EDC) were purchased from TCI Europe. $K_2HPO_4$ and NaCl were purchase from Carl Roth. All solutions were prepared using deionized water. The phosphate buffer saline (PBS) contains 0.1 M NaCl and 10 mM phosphate buffer (pH = 7.4).

Square-wave voltammetry (SWV) curves, cyclic voltammetry, and electrochemical impedance spectroscopy (EIS) were measured with the Reference 600 electrochemical station (Gamry Instruments Inc, USA). A three-electrode system was made up of a glassy carbon electrode (GCE, 4 mm in diameter) as the working electrode, an Ag/AgCl electrode (saturated KCl) as reference electrode, and a Pt wire as the counter electrode. Fourier-transform infrared (FT-IR) spectrum was obtained by the Nicolet™ iS50 FTIR Spectrometer (Thermo Fisher Scientific inc., USA). Scanning electron microscope (SEM) images were determined by JSM-7001F scanning electron microscope. Energy-dispersive X-ray spectroscopy (EDS) pictures were obtained by JEOL ISM-IT100. The micro flow SEC-MS setup was performed on the UltiMate RSLCnano system (Thermo Fisher Scientific, Breda, The Netherlands) and QExactive-Plus Hybrid Quadrupole-Orbitrap mass spectrometer (Thermo Fisher Scientific, Bremen, Germany).

### 2.5.2. Expression and purification of the enzyme variant UOx R298C

The synthetic gene encoding for the urate oxidase variant R298C from *Bacillus sp.* TB-90[4,17,38] (in the main manuscript referred as engUOx) was subcloned into a pET21a(+) plasmid between NdeI and XhoI restriction sites. The sequence contained a flexible linker (LQNAPAHG) before the XhoI site. *E. coli* BL21(DE3) cells were used as the host organism.

The UOx R298C expression and purification were performed according to the following procedure: For recombinant expression, 800 mL of lysogeny broth (LB) medium supplemented with ampicillin (100 µg/mL) were inoculated with 15 mL of an overnight culture harboring the desired plasmid DNA. Cells were grown at 37 °C until an $OD_{600}$ of 0.8-0.9 was reached, and the protein expression was induced by the addition of IPTG (0.5 mM). Protein expression was carried out overnight at 25 °C. After harvesting of the cells (4 °C, 8 × $10^3$ rpm, 10 min), the remaining cell pellet was resuspended in lysis buffer (50 mM $KH_2PO_4$, 300 mM NaCl, 10 mM imidazole, pH 8.0) prior to cell disruption by ultrasonication. The protein purification was performed by Ni-NTA affinity chromatography using pre-packed Ni-NTA HisTrap HP columns (GE Healthcare), previously equilibrated with lysis buffer. After loading of the filtered lysate, the column was washed with sufficient amounts of washing buffer (50 mM $KH_2PO_4$, 300 mM NaCl, 25 mM imidazole, pH 8.0), and bound protein was recovered with elution buffer (50 mM $KH_2PO_4$, 300 mM NaCl, 200 mM imidazole, pH 8.0). After SDS-PAGE, fractions containing the desired proteins in a sufficient purity (>90%) were pooled and dialyzed against 50 mM $K_2HPO_4/KH_2PO_4$ buffer (pH 8) overnight and concentrated using Centripreps (Millipore). The purified enzyme solution was stored at -80 °C as aliquots after shock-freezing in liquid nitrogen. The final concentration of the protein was determined at 280 nm ($\varepsilon_{280}$ = 36390 $M^{-1}$ $cm^{-1}$). A typical protein yield of 75 mg $L^{-1}$ cell culture was obtained.

### 2.5.3. Activity test for UOx R298C

The enzyme was tested for its activity by following the decrease in the absorbance of uric acid at 291 nm (ε = 12200 $M^{-1}$ $cm^{-1}$) as described in reference[4] at room temperature. The reaction mixture contained buffer (KPi, 50 mM, pH 8), uric acid (120 µM, added as a 5 mM stock in buffer) and enzyme (0.92 and 0.46 µM, respectively). The enzyme had a $k_{cat}$ value of 23 $min^{-1}$ under these conditions.

### 2.5.4. Electrodeposition of gold nanoparticle (AuNPs) on glass-carbon electrode (GCE)

Before modification, the GCE was polished with polishing film and washed by sonication in ultrapure water and ethanol for 1 min, respectively. The electrodepositing solution was prepared by using a 0.1 M KCl solution to dilute a 100 mM $HAuCl_4•3H_2O$ solution to obtain a 1 mM $HAuCl_4•3H_2O$ solution[39]. Subsequently, the electrodeposition of AuNPs on GCE was performed by cyclic voltammetry (CV) technique in the range between 0.2 and 1 V with a scan rate of 50 mV $s^{-1}$ in the above electrodepositing solution. Finally, the AuNPs deposited GCE (AuNPs/GCE) was washed by ultrapure water to remove the residual solution and then dried in air at room temperature.

### 2.5.5. Fabrication of the UA biosensing platform under the optimized condition

20 μL of a 2 mM aqueous solution of thioglycolic acid were incubated on AuNPs/GCE at 25 °C for 1 h and then washed with deionized water. Next, 50 μL of a 400 mM EDC solution was mixed with a 100 mM NHS solution, and the resulting mixture was dropped on the thioglycolic acid/AuNPs/GCE at 25 °C for 30 min to activate the carboxylic group of thioglycolic acid. The modified electrode was washed several times by ultrapure water to remove the residual solution. Then, 20 μL of a 1 mg $ml^{-1}$ UOx R298C solution was dropped on the surface of the modified electrode at 37 °C. After 2 h, the modified electrode was washed with deionized water to remove the excess of UOx R298C. Finally, 20 μL of a 200 μM GSH solution was dropped on the biosensing interface; then, the electrode was kept at 37 °C for 60 min. After that, the electrode was washed with deionized water.

### 2.5.6. General procedure for electrochemical measurements using UA biosensor

10 μL of a BSA solution was mixed with 10 μL of a UA solution at different concentrations. The mixture was incubated on the biosensing interface at 37 °C for 2 h. After being rinsed by deionized water, the resulted electrodes were measured in a 5 mM $[Fe(CN)_6]^{3-/4-}$ and 0.1 M KCl aqueous solution by square wave voltammetry (SWV) in the range from -0.2 to 0.6 V with pulse amplitude of 25 mV and an increased potential of 4 mV.

### 2.5.7. Selectivity property of UA biosensor

10 μL of interferent solution and UA solution were dropped on the constructed UA biosensing platform, respectively. Then, 0.1% BSA solution was incubated with the above solution on the electrodes for 2 h at 37 °C. The concentrations of interferents were: AA (1 mM), dopamine (1 mM), Glu (1 mM), GSH (1 mM), l-Cys (1 mM), urea (1 mM) and thioglycolic acid (1 mM), respectively. The mixture contains all these interferents (1 mM, each) and UA (0.1 mM). Finally, the electrochemical signal was read out in a 5 mM $[Fe(CN)_6]^{3-/4-}$ and 0.1 M KCl solution by square wave voltammetry (SWV) in the range from -0.2 to 0.6 V with pulse amplitude of 25 mV and an increased potential of 4 mV. After each incubation steps, the electrodes were washed with ultra-pure water.

### 2.5.8. Micro-flow SEC-MS to study GSH binding to BSA

The binding of GSH to BSA under oxidative conditions was studied using native microflow SEC-MS methods[40]. The samples were prepared by incubation of aqueous solutions of $H_2O_2$ (250 μL, 1 mM), BSA (250 μL, 10 mg $mL^{-1}$) and GSH (500 μL, 200

μM) in Eppendorf tubes, at 37 °C, for 2 h and in an orbital shaker (170 rpm). Therefore, the final volume was 1 mL (final concentrations of BSA, $H_2O_2$ and GSH in the reaction solution were 2.5 mg $mL^{-1}$, 250 μM and 100 μM respectively). A 200 mM ammonium acetate was employed as the dilution solvent when they were analyzed. For the microflow SEC part, the measurement was conducted by TSK gel Super SW3000 (1.0 × 300 mm × 4 μm, TOSOH, Japan) column at a flow rate of 15 μL $min^{-1}$ with 200 mM ammonium acetate as mobile phase, and 1 μL as injection volume. The MS spectrum was acquired with HRM-AIF mode. The parameters were as follows. Polarity: positive. In-source CID: 50 eV. Microscans: 10. Resolution: 17500. Maximum injection time: 200 ms. Scan range: 350 to 6000. AGC target: $3\times10^6$. Capillary temperature: 275 ° C. Sheath gas flow: 15. Auxiliary gas flow: 5. Spray voltage: 2.5 kV. S-lens RF level: 200. The MS data was visualized with FreeStyle 1.6 software (Thermo Fisher Scientific). The deconvolution results were carried out with UniDec software (University of Arizona, Phoenix, AZ, USA)[41].

### 2.5.9. Sequence alignment between engUOx and commercially available UOx from Candida sp.

Unfortunately, the amino acid sequence of the commercial UOx from Candida sp. (Sigma-Aldrich) is not available. Therefore, a structural comparison, even via homology modeling, is not possible. However, judging from past literature, the amino acid sequence of UOx from *Candida sp.* (Sigma-Aldrich) must be similar to the sequence of the UOx from *Candida utilis*.[14] An amino acid sequence alignment between engUOx (i.e., *Bacillus sp.* TB-90)[1,2] and UOx from *Candida utilis*[14] reveals a very low sequence identity.

Sequence 1 is engUOx (i.e. *Bacillus sp.* TB-90).
Sequence 2 is UOx from *Candida utilis*.

The percentage of sequence identity is only 24%.

```
CLUSTAL O(1.2.4) multiple sequence alignment


sequence1      TKHKERVMYYGKGDVFAYRTYLKPLTGVRTIPESPFSGRDHILFGVNVKISVGGTKLLTS     60
sequence2      MSTTLSSSTYGKDNVKFL--------KVKKDPQNP---KKQEVMEATVTCL-LEGGFDTS     48
                . .     ***.:*           *:. *:.*   :.: :: ..*.       : **

sequence1      FTKGDNSLVVATDSMKNFIQKHLASYTGTTIEGFLEYVATSFLKKYSHIEKISLIGE---     117
sequence2      YTEADNSSIVPTDTVKNTILVLAKTTEIWPIERFAAKLATHFVEKYSHVSGVSVKIVQDR     108
               :*:.*** :* **::** *     :     ** *   :** *::****:. :*:

sequence1      -------EIPFETTFAVKNGNRAASELVFKKSRNEYATAYLNMVRNEDNTLNITEQQSGL     170
sequence2      WVKYAVDGKPHDHSFIHEGGEKRITDLYYKRSGD-------------------YKLSSAI     149
                     *.: :*  :.*::  ::* :*:* :                    : .*.:

sequence1      AGLQLIKVSGNSFVGFIRDEYTTLPEDSNRPLFVYLNIKWKYKNTEDSFGTNPENY----     226
sequence2      KDLTVLKSTGSMFYGYNKCDFTTLQPTTDRILSTDVDATWVWDNKKIGSVYDIAKAADKG     209
                .* ::* :*. * *: : ::***   ::* * . :: .* :.*.: .   :  :

sequence1      ---VAAEQIRDIATSVFHETETLSIQHLIYLIGRRILERFPQLQEVYFESQ-------NH     276
sequence2      IFDNVYNQAREITLTTFALENSPSVQATMFNMATQILEKACSVYSVSYALPNKHYFLIDL     269
                   . :* *:*: :.*   :: *:*  :: :. :***:  .: .* :          :

sequence1      TWDKIVEEIPESEGKVYTEPCPPYGFQCFTVTQEDLPHENILMFSDEPDHKGALK  331
sequence2      KWKGL----ENDNELFYPSPHPNGLIKCTVVRKEKTKL----------------  303
               .*. :     :.:  .* .* *   ::* .* :*.
```

## 2.6. References

[1] Chen, H., Simoska, O., Lim, K., Grattieri, M., Yuan, M., Dong, F., Lee, Y. S., Beaver, K., Weliwatte, S., Gaffney, E. M. & Minteer, S. D. Fundamentals, applications, and future directions of bioelectrocatalysis. *Chem. Rev.* **120**, 12903-12993, https://doi.org/10.1021/acs.chemrev.0c00472 (2020).

[2] Chaibun, T., Puenpa, J., Ngamdee, T., Boonapatcharoen, N., Athamanolap, P., O'Mullane, A. P., Vongpunsawad, S., Poovorawan, Y., Lee, S. Y. & Lertanantawong, B. Rapid electrochemical detection of coronavirus SARS-CoV-2. *Nat. Commun.* **12**, 802, https://doi.org/10.1038/s41467-021-21121-7 (2021).

[3] Liu, Y., Wei, Z., Zhou, J. & Ma, Z. Simultaneous multi-signal quantification for highly precise serodiagnosis utilizing a rationally constructed platform. *Nat. Commun.* **10**, 5361, https://doi.org/10.1038/s41467-019-13358-0 (2019).

[4] Hibi, T., Hayashi, Y., Fukada, H., Itoh, T., Nago, T. & Nishiya, Y. Intersubunit salt bridges with a sulfate anion control subunit dissociation and thermal stabilization of Bacillus sp. TB-90 urate oxidase. *Biochemistry* **53**, 3879-3888, https://doi.org/10.1021/bi500137b (2014).

[5] Ding, S., Lyu, Z., Fang, L., Li, T., Zhu, W., Li, S., Li, X., Li, J. C., Du, D. & Lin, Y. Single-atomic site catalyst with heme enzymes-like active sites for electrochemical sensing of hydrogen peroxide. *Small* **17**, e2100664, https://doi.org/10.1002/smll.202100664 (2021).

[6] Liang, W., Wied, P., Carraro, F., Sumby, C. J., Nidetzky, B., Tsung, C. K., Falcaro, P. & Doonan, C. J. Metal-organic framework-based enzyme biocomposites. *Chem. Rev.* **121**, 1077-1129, https://doi.org/10.1021/acs.chemrev.0c01029 (2021).

[7] Tang, C., Saquing, C. D., Morton, S. W., Glatz, B. N., Kelly, R. M. & Khan, S. A. Cross-linked polymer nanofibers for hyperthermophilic enzyme immobilization: approaches to improve enzyme performance. *ACS Appl. Mater. Interfaces* **6**, 11899-11906, https://doi.org/10.1021/am5033633 (2014).

[8] Li, M., Qiao, S., Zheng, Y., Andaloussi, Y. H., Li, X., Zhang, Z., Li, A., Cheng, P., Ma, S. & Chen, Y. Fabricating covalent organic framework capsules with commodious microenvironment for enzymes. *J. Am. Chem. Soc.* **142**, 6675-6681, https://doi.org/10.1021/jacs.0c00285 (2020).

[9] Singh, R., Musameh, M., Gao, Y., Ozcelik, B., Mulet, X. & Doherty, C. M. Stable MOF@enzyme composites for electrochemical biosensing devices. *J. Mater. Chem. C* **9**, 7677-7688, https://doi.org/10.1039/d1tc00407g (2021).

[10] Musil, M., Konegger, H., Hon, J., Bednar, D. & Damborsky, J. Computational Design of stable and soluble biocatalysts. *ACS Catal.* **9**, 1033-1054, https://doi.org/10.1021/acscatal.8b03613 (2018).

[11] Wijma, H. J., Floor, R. J., Jekel, P. A., Baker, D., Marrink, S. J. & Janssen, D. B. Computationally designed libraries for rapid enzyme stabilization. *Protein Eng. Des. Sel.* **27**, 49-58, https://doi.org/10.1093/protein/gzt061 (2014).

[12] Bommarius, A. S. & Paye, M. F. Stabilizing biocatalysts. *Chem. Soc. Rev.* **42**, 6534-6565, https://doi.org/10.1039/c3cs60137d (2013).

[13] Romero-Rivera, A., Garcia-Borras, M. & Osuna, S. Computational tools for the evaluation of laboratory-engineered biocatalysts. *Chem. Commun.* **53**, 284-297, https://doi.org/10.1039/c6cc06055b (2016).

[14] Planas-Iglesias, J., Marques, S. M., Pinto, G. P., Musil, M., Stourac, J., Damborsky, J. & Bednar, D. Computational design of enzymes for biotechnological applications. *Biotechnol. Adv.* **47**, 107696, https://doi.org/10.1016/j.biotechadv.2021.107696 (2021).

[15] Tseliou, V., Knaus, T., Masman, M. F., Corrado, M. L. & Mutti, F. G. Generation of amine dehydrogenases with increased catalytic performance and substrate scope from epsilon-deaminating L-Lysine dehydrogenase. *Nat. Commun.* **10**, 3717, https://doi.org/10.1038/s41467-019-11509-x (2019).

[16] Knaus, T., Paul, C. E., Levy, C. W., de Vries, S., Mutti, F. G., Hollmann, F. & Scrutton, N. S. Better than nature: nicotinamide biomimetics that outperform natural coenzymes. *J. Am. Chem. Soc.* **138**, 1033-1039, https://doi.org/10.1021/jacs.5b12252 (2016).

[17] Hibi, T., Kume, A., Kawamura, A., Itoh, T., Fukada, H. & Nishiya, Y. Hyperstabilization of tetrameric *Bacillus sp.* TB-90 urate oxidase by introducing disulfide bonds through structural plasticity. *Biochemistry* **55**, 724-732, https://doi.org/10.1021/acs.biochem.5b01119 (2016).

[18] Ghosh, T., Sarkar, P. & Turner, A. P. A novel third generation uric acid biosensor using uricase electro-activated with ferrocene on a Nafion coated glassy carbon electrode. *Bioelectrochemistry* **102**, 1-9, https://doi.org/10.1016/j.bioelechem.2014.11.001 (2015).

[19] Yang, M., Wang, H., Liu, P. & Cheng, J. A 3D electrochemical biosensor based on Super-Aligned Carbon NanoTube array for point-of-care uric acid monitoring. *Biosens. Bioelectron.* **179**, 113082, https://doi.org/10.1016/j.bios.2021.113082 (2021).

[20] Lu, X., Li, S., Guo, W., Zhang, F. & Qu, F. A covalent organic polymer-TiO(2)/Ti(3)C(2) heterostructure as nonenzymatic biosensor for voltammetric detection of dopamine and uric acid. *Microchim. Acta* **188**, 95, https://doi.org/10.1007/s00604-021-04755-8 (2021).

[21] Chauvin, J. R. & Pratt, D. A. On the Reactions of Thiols, Sulfenic Acids, and Sulfinic Acids with Hydrogen Peroxide. *Angew. Chem. Int. Ed.* **56**, 6255-6259, https://doi.org/10.1002/anie.201610402 (2017).

[22] Takashio, M., Chikano, T. & Kamimura, M. Uricase and a method for the preparation thereof. US4882280 (1992).

[23] Zhang, D., Li, W. & Ma, Z. Improved sandwich-format electrochemical immunosensor based on "smart" $SiO_2$@polydopamine nanocarrier. *Biosens. Bioelectron.* **109**, 171-176, https://doi.org/10.1016/j.bios.2018.03.027 (2018).

[24] Desideri, G., Castaldo, G., Lombardi, A., Mussap, M., Testa, A., Pontremoli, R., Punzi, L. & Borghi, C. Is it time to revise the normal range of serum uric acid levels? *Eur. Rev. Med. Pharmacol. Sci.* **18**, 1295-1306 (2014).

[25] Huang, C. T., Chen, M. L., Huang, L. L. & Mao, I. F. Uric acid and urea in human sweat. *Chin. J. Physiol.* **45**, 109-115 (2002).

[26] Qu, S., Li, Z. & Jia, Q. Detection of purine metabolite uric acid with picolinic-acid-functionalized metal-organic frameworks. *ACS Appl. Mater. Interfaces* **11**, 34196-34202, https://doi.org/10.1021/acsami.9b07442 (2019).

[27] Jain, S., Verma, S., Singh, S. P. & Sharma, S. N. An electrochemical biosensor based on novel butylamine capped CZTS nanoparticles immobilized by uricase for uric acid detection. *Biosens. Bioelectron.* **127**, 135-141, https://doi.org/10.1016/j.bios.2018.12.008 (2019).

[28] Galliani, M., Diacci, C., Berto, M., Sensi, M., Beni, V., Berggren, M., Borsari, M., Simon, D. T., Biscarini, F. & Bortolotti, C. A. Flexible printed organic electrochemical transistors for the detection of uric acid in artificial wound exudate. *Adv. Mater. Interfaces* **7**, 2001218, https://doi.org/ARTN 200121810.1002/admi.202001218 (2020).

[29] Wang, K., Wu, C., Wang, F., Liao, M. & Jiang, G. Bimetallic nanoparticles decorated hollow nanoporous carbon framework as nanozyme biosensor for highly sensitive electrochemical sensing of uric acid. *Biosens. Bioelectron.* **150**, 111869, https://doi.org/10.1016/j.bios.2019.111869 (2020).

[30] Ahmad, R., Tripathy, N., Jang, N. K., Khang, G. & Hahn, Y. B. Fabrication of highly sensitive uric acid biosensor based on directly grown ZnO nanosheets on electrode surface. *Sens. Actuator B-Chem.* **206**, 146-151, https://doi.org/10.1016/j.snb.2014.09.026 (2015).

[31] Shi, W. *et al.* An electrochemical biosensor based on multi-wall carbon nanotube-modified screen-printed electrode immobilized by uricase for the detection of salivary uric acid. *Anal. Bioanal. Chem.* **412**, 7275-7283, https://doi.org/10.1007/s00216-020-02860-w (2020).

[32] Abbas, M. W., Soomro, R. A., Kalwar, N. H., Zahoor, M., Avci, A., Pehlivan, E., Hallam, K. R. & Willander, M. Carbon quantum dot coated $Fe_3O_4$ hybrid composites for sensitive electrochemical detection of uric acid. *Microchem. J.* **146**, 517-524, https://doi.org/10.1016/j.microc.2019.01.034 (2019).

[33] Feng, J., Liang, X. & Ma, Z. New immunoprobe: Dual-labeling ZIF-8 embellished with multifunctional bovine serum albumin lamella for electrochemical immunoassay of tumor marker. *Biosens. Bioelectron.* **175**, 112853, https://doi.org/10.1016/j.bios.2020.112853 (2021).

[34] Liu, J. L., Zhuo, Y., Chai, Y. Q. & Yuan, R. BSA stabilized tetraphenylethylene nanocrystals as aggregation-induced enhanced electrochemiluminescence emitters for ultrasensitive microRNA assay. *Chem. Commun.* **55**, 9959-9962, https://doi.org/10.1039/c9cc04660g (2019).

[35] Lin, Y., Zhou, Q. & Tang, D. Dopamine-loaded liposomes for in-situ amplified photoelectrochemical immunoassay of AFB(1) to enhance photocurrent of $Mn^{2+}$-Doped $Zn_3(OH)_2V_2O_7$ Nanobelts. *Anal. Chem.* **89**, 11803-11810, https://doi.org/10.1021/acs.analchem.7b03451 (2017).

[36] Qian, Y., Zhang, L. & Tian, Y. Highly Stable Electrochemical Probe with Bidentate Thiols for Ratiometric Monitoring of Endogenous Polysulfide in Living Mouse Brains. *Anal. Chem.* **94**, 1447-1455, https://doi.org/10.1021/acs.analchem.1c04894 (2022).

[37]Tao, L., Li, D., Li, Y., Shi, X., Wang, J., Rao, C. & Zhang, Y. Designing a mutant Candida uricase with improved polymerization state and enzymatic activity. *Protein Eng. Des. Sel.* **30**, 753-759, https://doi.org/10.1093/protein/gzx056 (2017).

[38] Masachika Takashio, Y. T. C., S.; Minoru Kamimura, Y. Uricase and a method for the preparation thereof. US4882280 (1989).

[39] Zhang, D. S., Li, W. X. & Ma, Z. F. Improved sandwich-format electrochemical immunosensor based on "smart" $SiO_2$@polydopamine nanocarrier. *Biosens. Bioelectron.* **109**, 171-176, https://doi.org/10.1016/j.bios.2018.03.027 (2018).

[40] Ventouri, I. K., Veelders, S., Passamonti, M., Endres, P., Roemling, R., Schoenmakers, P. J., Somsen, G. W., Haselberg, R. & Gargano, A. F. G. Micro-flow size-exclusion chromatography for enhanced native mass spectrometry of proteins and protein complexes. *Anal. Chim. Acta* **1266**, 341324, https://doi.org/10.1016/j.aca.2023.341324 (2023).

[41] Marty, M. T., Baldwin, A. J., Marklund, E. G., Hochberg, G. K., Benesch, J. L. & Robinson, C. V. Bayesian deconvolution of mass and ion mobility spectra: from binary interactions to polydisperse ensembles. *Anal. Chem.* **87**, 4370-4376, https://doi.org/10.1021/acs.analchem.5b00140 (2015).